International Journal of Mechanical, Industrial and Aerospace Sciences
ISSN: 2517-9950
Vol:6, No:1, 2012

Numerical Analysis of the Influence of Airfoil Asymmetry on VAWT Performance

Marco Raciti Castelli, Giulia Simioni and Ernesto Benini

***Abstract*—**This paper presents a model for the evaluation of energy performance and aerodynamic forces acting on a three-bladed small vertical axis Darrieus wind turbine depending on blade chord curvature with respect to rotor axis.

The adopted survey methodology is based on an analytical code coupled to a solid modeling software, capable of generating the desired blade geometry depending on the blade design geometric parameters, which is linked to a finite volume CFD code for the calculation of rotor performance.

After describing and validating the model with experimental data, the results of numerical simulations are proposed on the bases of two different blade profile architectures, which are respectively characterized by a straight chord and by a curved one, having a chord radius equal to rotor external circumference. A CFD campaign of analysis is completed for three blade-candidate airfoil sections, that is the recently-developed DU 06-W-200 cambered blade profile, a classical symmetrical NACA 0021 and its derived cambered airfoil, characterized by a curved chord, having a chord radius equal to rotor external circumference.

The effects of blade chord curvature on angle of attack, blade tangential and normal forces are first investigated and then the overall rotor torque and power are analyzed as a function of blade azimuthal position, achieving a numerical quantification of the influence of blade camber on overall rotor performance.

***Keywords*—**VAWT, NACA 0021, DU 06-W-200, cambered airfoil

I. Introduction and Background

THE vertical axis wind turbine has an inherently non-stationary aerodynamic behavior, mainly due to the continuous variation of the blade angle of attack during the rotation of the machine: this peculiarity involves the continuous variation both of the relative velocity with respect to the blade profile and - although to a lesser extent - of the corresponding Reynolds number. This phenomenon, typical of slow rotating machines, has a significant effect both on the dynamic loads acting on the rotor and on the generated power and, therefore, on performance.

Classical aerodynamic tools such as the theory of blade elements (BE-M), while presenting the certain advantage of low computation times, are nevertheless limited by the availability of extended airfoil databases (up to 180°) which should also refer to rather low local Reynolds numbers (close to Re = 10^5), which are typical of vertical axis wind turbines operation. The airfoil section data requirements for application to vertical axis wind turbines are in fact broader in scope than are those the aircraft industry usually concerns itself with.

Since most airfoil databases which are available in the literature are derived from aeronautical applications, hardly extending beyond stall and also referring to relatively high Reynolds numbers (above Re = 10^6), it has been recognized that there is a paucity of accurate airfoil data needed to describe the aerodynamics of wind turbine blades. This limits vertical axis wind turbine classical analysis to a narrow number of blade profiles, substantially some NACA series symmetrical airfoil, for which low Reynolds numbers extended databases are available in technical literature [1].

Until now high quality wind tunnel data is required to verify the aerodynamic design of a rotor, in order to obtain the operating torque curves for the implementation of the control system. Advanced computational methods could nevertheless provide a highly efficient means of maturing initial concept studies into effective aerodynamic designs that meet target operational objectives. Nevertheless, Computational Fluid Dynamics (CFD) can nowadays be considered as a powerful design tool, whose integration into industrial development and production life-cycles is continuously rising. In CFD simulations, the computer essentially replaces the physical simulation in the wind tunnel. CFD methods involve very large amounts of computation even for relatively simple problems and their accuracy is often difficult to assess when applied to a new problem where prior experimental validation has not been done [2]. Anyway, performing CFD calculations provide knowledge about the flow in all its details, such as velocities, pressure, temperature, etc. Further, all types of useful graphical presentations, such as flow lines, contour lines and iso-lines are readily available. This stage can be compared to having completed a wind-tunnel study or an elaborate full-scale measurement campaign [3].

The limitations in low Reynolds number accurate aerodynamic databases can be overcame by the use of CFD codes which can outflank the lack of airfoil data thanks to their inherent ability to determine the aerodynamic components of actions through the integration of the Navier-Stokes equations in the neighborhood of the wind turbine blade profile.

Marco Raciti Castelli is Research Associate at the Department of Mechanical Engineering of the University of Padua, Via Venezia 1, 35131 Padova, Italy (e-mail: marco.raciticastelli@unipd.it).

Giulia Simioni is M.Sc. Student in Aerospace Engineering at the Politecnico di Torino, Via Duca degli Abruzzi 24, 10129 Torino, Italy (e-mail: giulia.simioni@libero.it).

Ernesto Benini is Associate Professor at the Department of Mechanical Engineering of the University of Padua, Via Venezia 1, 35131 Padova, Italy (e-mail: ernesto.benini@unipd.it).

Up to now, blade camber effects on the performance of Darrieus model micro vertical axis wind turbines have not been extensively investigated [4]. Some experimental tests have been conducted in the Eighties at Sandia National Laboratories, showing some improvements of almost all rotor performance characteristics [5]. Anyway, as reported by Saeed et al., scarcity of airfoil aerodynamic characteristics data still limit the choice of candidate airfoil sections to a few [6]. Though the adoption of cambered airfoil sections for increased performance has been suggested by several investigators [7] [8], the design choice of a cambered blade section as a mean of improving overall rotor performance remains to be further investigated.

In this paper, a CFD campaign of analysis was completed for three blade-candidate airfoil sections:

- the recently-developed DU 06-W-200 cambered blade profile;
- a classical symmetrical NACA 0021;
- a cambered airfoil, derived from the NACA 0021 and characterized by a curved chord, having a chord radius equal to rotor external circumference for a rotor having a value of chord to radius ratio, defined as:

$$c_R = c/R \quad (1)$$

equal to 0.17.

II. Model Geometry

Fig. 1 shows a schema of the adopted survey methodology, consisting in the coupling of an analytical code to a solid modeling software, capable of generating the desired blade geometry depending on the desired design geometric parameters, which is linked to a finite volume CFD code for the calculation of rotor performance.

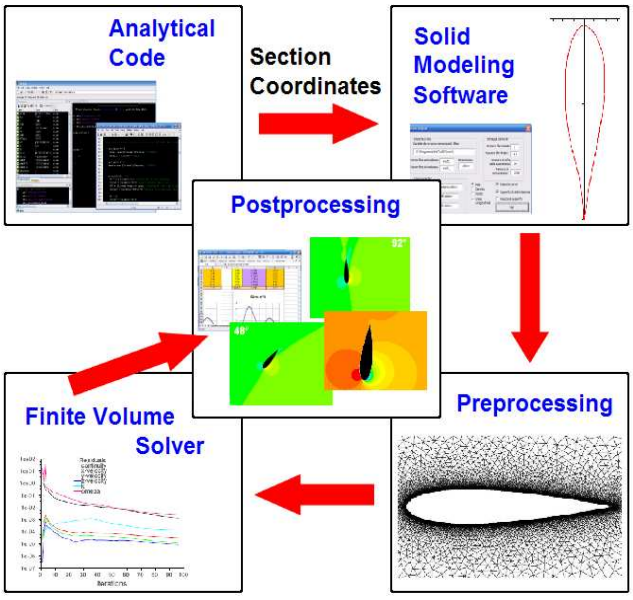

Fig. 1 Schema of the survey methodology

The aim of this work was to numerically analyze the aerodynamic behavior of a 2D vertical-axis three-bladed Darrieus wind turbine characterized by three different blade profile sections, which are summarized in Table 1.

TABLE I
Main features of the three tested airfoil sections

Blade section	c [mm]
NACA 0021	85.8
cambered NACA 002	85.8
DU 06-W-200	85.8

The common features of the tested rotors are summarized in Table II. The solidity parameter σ is defined as Nc/R, as suggested by Strickland [9].

TABLE II
Common features of the tested rotors

D [mm]	1030
H [mm]	1 (2D simulation)
N [-]	3
Spoke-blade connection	0.25 c
σ [-]	0.5

Fig. 2 displays the analytical design process of a cambered generic blade section having a chord radius equal to rotor external circumference.

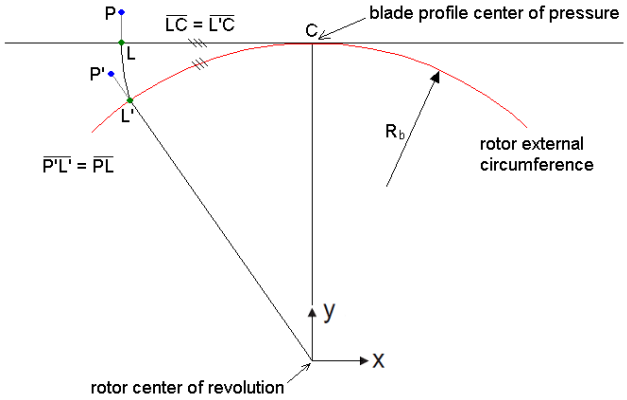

Fig. 2 Analytical design process of a cambered generic blade section. The length of the segment LC is equal to that of the curved segment L'C

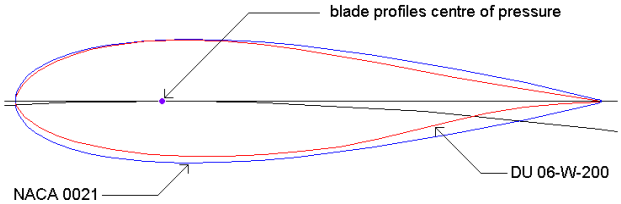

Fig. 3 Comparison between the classical NACA 0021 blade section (blue) and DU 06-W-200 blade section (red)

Figs. 3, 4 and 5 compare the geometries of the classical NACA 0021 with the corresponding cambered geometry and

with DU 06-W-200 blade section. The chord radius R_b with respect to rotor axis was set equal to the rotor radius R.

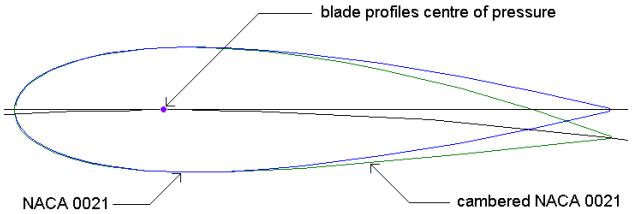

Fig. 4 Comparison between the classical NACA 0021 blade section (blue) and the corresponding cambered section (green)

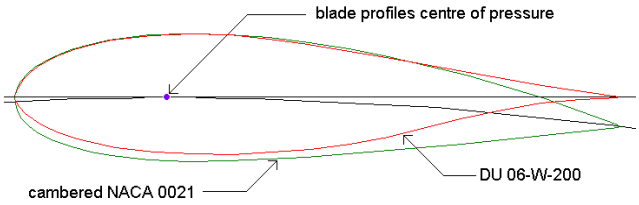

Fig. 5 Comparison between cambered NACA 0021 blade section (green) and DU 06-W-200 blade section (red)

The blade azimuthal position was identified by the angular coordinate of the pressure centre of the blade midsection, as can be seen in Fig. 6.

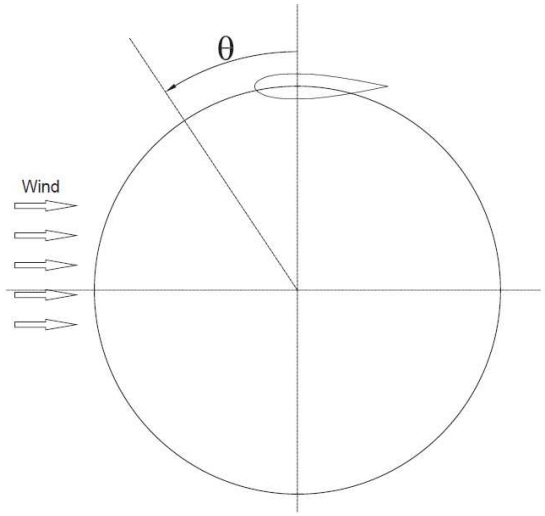

Fig. 6 Blade azimuthal coordinate

III. Spatial Domain Discretization

All the meshes which were adopted in the present work had common geometric features, except for the areas close to the blade profiles.

As the aim of the present work was to reproduce the operation of a rotating machine, the use of moving sub-grids was necessary. In particular, the discretization of the computational domain into macro-areas led to two distinct sub-grids:

- a rectangular outer zone, determining the overall calculation domain, with a circular opening centered on the turbine rotational axis, which was identified as Wind Tunnel sub-grid, fixed;
- a circular inner zone, which was identified as Rotor sub-grid, revolving with rotor angular velocity ω.

A. Wind Tunnel sub-grid

Fig. 7 shows the main dimensions and the boundary conditions of the Wind Tunnel sub-grid area.

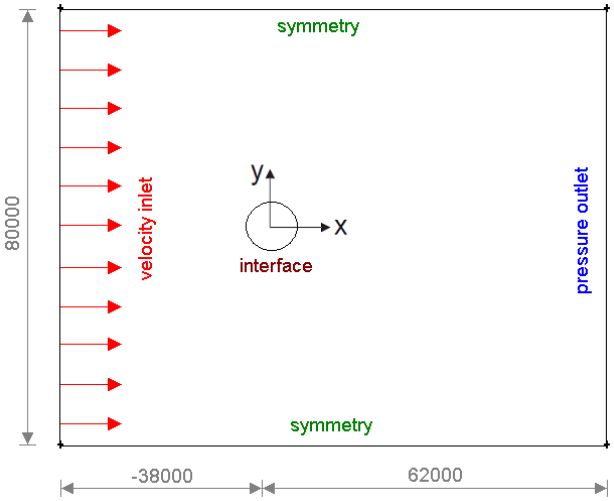

Fig. 7 Main dimensions [mm] of the Wind Tunnel sub-grid area

Inlet and outlet boundary conditions were placed respectively 37 rotor diameters upwind and 60 rotor diameters downwind with respect to the rotor, allowing a full development of the wake, in accordance to what suggested by the work of Ferreira et al [10].

The computational domain width was set almost 80 rotor diameters so that the value of solid blockage, calculated according to Mercker [11] was less than 0.32% and would cause an increase in the cube of the velocity at the test section of less than 1% with respect to the value of unperturbed wind velocity at computational domain entrance, in formulas:

$$\varepsilon_{sb} = ¼\,(D \cdot H)/(W_{domain} \cdot H_{domain}) \quad (2)$$

$$V_{test\ section} = (1+ \varepsilon_{sb})V_{\infty} \quad (3)$$

Since the estimation of the correct value of wake blockage was rather difficult, and being the overall calculation domain oversized by imposing the requirement on the cube of the velocity at the test section, the wake blockage was not considered in these calculations.

Two *symmetry* boundary condition were used for the two side walls. The circumference around the circular opening centered on the turbine rotational axis was set as an *interface*, thus ensuring the continuity of the flow field.

An unstructured mesh was chosen for the Wind Tunnel sub-grid, in order to reduce engineering time to prepare the CFD simulations.

B. Rotor sub-grid

The Rotor sub-grid is the fluid area simulating the rotation of the wind turbine and is therefore characterized by a moving mesh, rotating at the same angular velocity of the turbine. Its location coincides exactly with the circular opening inside the Wind Tunnel sub-grid area and centered on the turbine rotational axis.

Fig. 8 shows the main dimensions and the boundary conditions of the Wind Tunnel sub-grid area.

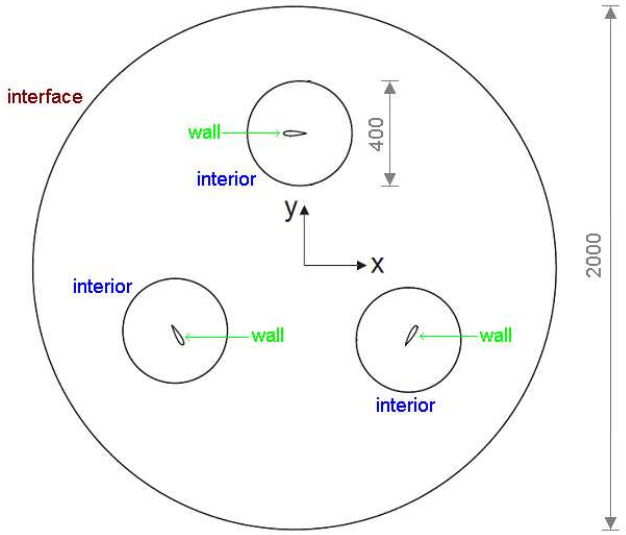

Fig. 8 Main dimensions [mm] of the Rotor sub-grid area

It is good engineering practice to provide that the mesh on both sides of the interface (Rotor sub-grid and Wind Tunnel sub-grid areas) has approximately the same characteristic cell size in order to obtain faster convergence [12].

An isotropic unstructured mesh was chosen for the Rotor sub-grid, in order to guarantee the same accuracy in the prediction of rotor's performance during the rotation – according to the studies of Commings et al. [13] – and also in order to test the prediction capability of a very simple grid. Considering their features of flexibility and adaption capability, unstructured meshes are in fact very easy to obtain, also for complex geometries, and often represent the "first attempt" in order to get a quick response from the CFD in engineering work.

All blade profiles inside the Rotor sub-grid are enclosed in a control circle of 400 mm diameter. Unlike the interface, it has no physical significance: its aim is to allow a precise dimensional control of the grid elements in the area close to rotor blades by adopting a first size function operating from the blade profile to the control circle itself and a second size function operating from the control circle to the whole Rotor sub-grid area, ending with grid elements of the same size of the corresponding Wind tunnel sub-grid elements. An interior boundary condition was used for control circle borders, thus ensuring the continuity of the cells on both sides of the mesh.
A growth factor of 1.26 was set from the surface of the control circle to Rotor sub-grid, thus expanding grid size from 4 mm to 10 mm, as shown in Fig. 9.

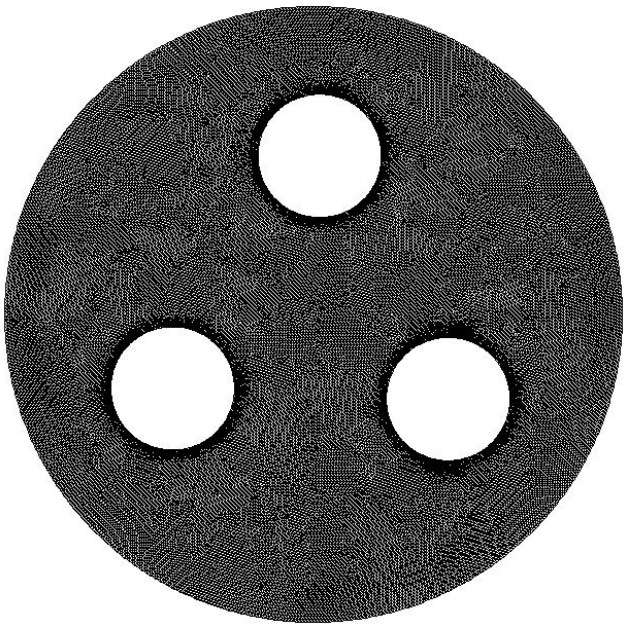

Fig. 9 Rotor sub-grid

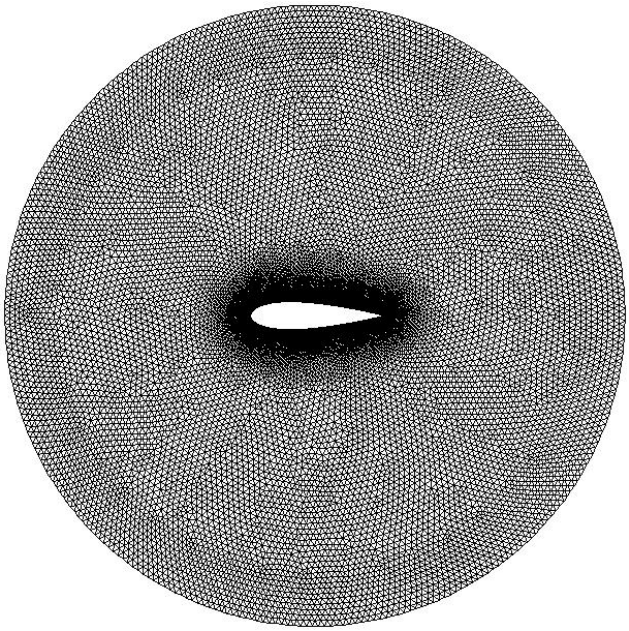

Fig. 10 Control circle for NACA 0021 blade section.

IV. The Contro Circle

Being the area close to the blade profiles, most attention was placed to the control circle. All the differences between

various meshes adopted in the present work were concentrated in this area.

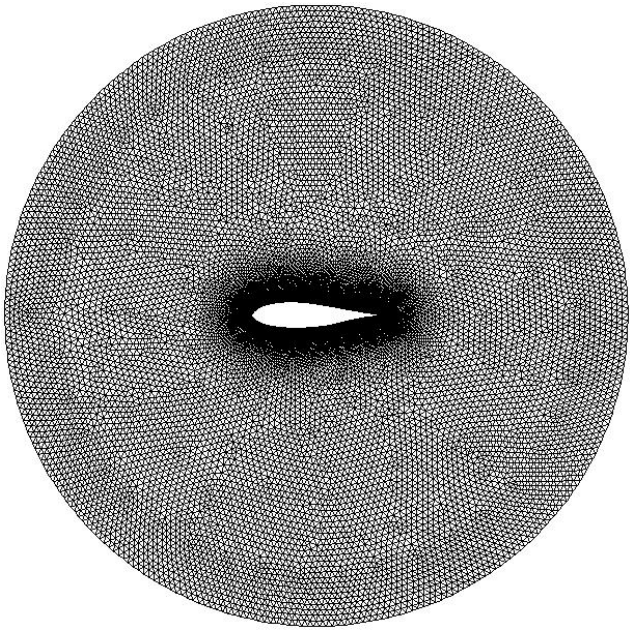

Fig. 11 Control circle for DU 06-W-200 blade section

The computational grids were constructed from lower topologies to higher ones, adopting appropriate size functions, in order to cluster grid points near the leading edge and the trailing edge of the blade profile, so as to improve the CFD code capability of determining lift, drag and the separation of the flow from the blades itself. Two size functions were set inside the control circle, as shown in Fig. 12.

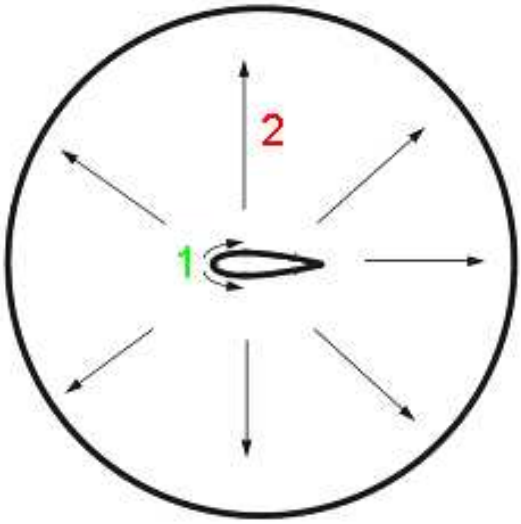

Fig. 12 Size functions applied to control circle elements

Size function No. 1 started from the leading edge and influences inner and outer blade profile. Size function No. 2 started from the blade profile and influences the whole control cylinder area, as described in the previous section.

The trailing edge thickness was set to about 0.38 mm, as shown in figure 13.

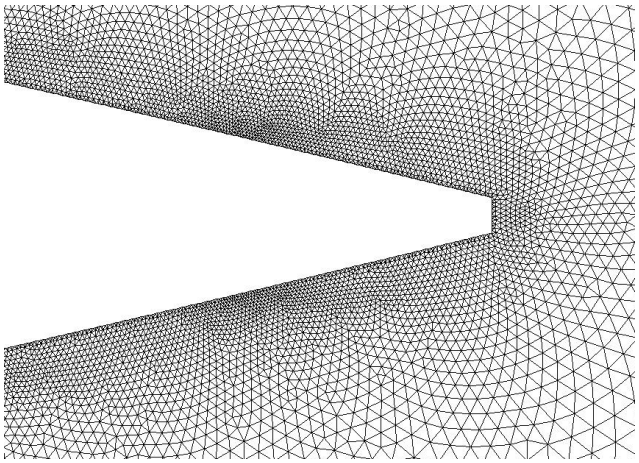

Fig. 13 Grid points clustering close to trailing edge for NACA 0021 blade section

V. Numerical Code Validation

Before analyzing the models described in the previous section, a complete validation work based on wind tunnel measurements was conducted [13]. The experimental setup consisted in a classical vertical-bladed Darrieus rotor made of aluminum and carbon fibers, using a NACA 0021 blade profile with a chord length of 85.8 mm, which was tested in Bovisa's low turbulence facility (Milan).

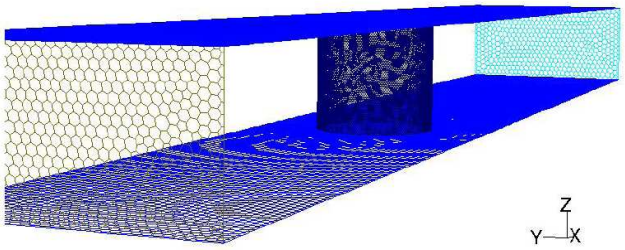

Fig. 14 Validation model, 3D computational domain

A computational domain of rectangular shape was been chosen, having the same wind tunnel external sizes: the wall boundary conditions of the model consisted in two lateral walls spaced 2000 mm apart from the wind tunnel centerline (the wind tunnel measured 4000 mm in width and 3880 mm in height). The rotor axis was placed on the symmetry position of the wind tunnel section. 2D and 3D simulations were performed, in order to take into account also the drag effect induced by the spokes. Only half of the experimental setup was modeled, due to its vertical symmetry: in this case a symmetry boundary condition was used. Anyway, the geometrical features of the model did not allow other simplifications to be performed. The effect of gravity on the rotor working curves

has not been contemplated, being considered not influential for the scope of this work.

Inlet and outlet boundary conditions were placed respectively 10 diameters upwind and 14 diameters downwind of the rotor, allowing a full development of the wake. The main features of the validation model are summarized in Table 3.

TABLE III
VALIDATION MODEL MAIN FEATURES

Profile type	NACA 0021
c [mm]	85.8
R [mm]	515
H [mm]	1456.4
A [m^2]	1.236
σ	0.25
Spoke-blade connection	0.5 c
Wind tunnel dimensions [mm]	4000 x 3800

The correction due to wind tunnel blockage was not applied, in order to minimize any possible source of error due to a wrong estimation of the blockage of the wind tunnel itself. Furthermore, this choice has the significant advantage of reducing the computational domain, allowing a saving in the total number of mesh elements. The correction of the friction resistive torque due to the bearings was taken into account.

In order to test the code sensitivity to the number of grid points, three unstructured meshes were adopted for the Rotor sub-grid, both for one-bladed and three-bladed configurations, while the Wind Tunnel sub-grid remained substantially the same. Table 4 shows mesh main characteristic for both one-bladed and three-bladed configurations.

TABLE IV
TWO-DIMENSIONAL MESH MAIN CHARACTERISTICS (VALIDATION MODEL)

	Mesh ID	Total mesh elements	Maximum near-blade grid dimension [mm]
1 blade	2 D		
	Mod 0'	9.1 · 105	0,050
	Mod A'	7.7 · 105	0,075
	Mod B'	6.3 · 105	0,100
3 blades	2 D		
	Mod 0'	1.3 · 106	0,050
	Mod A'	1.1 · 106	0,075
	Mod B'	9.0 · 105	0,100

After some corrections to take into account spoke drag, the average torque values measured in the wind tunnel for a 9 m/s wind speed and different tip speed ratios, were compared with those obtained from CFD analysis for three different grids (characterized by different blade size function values) and three different turbulence models (k-ω SST, k-ε Realizable and Spalart-Allmaras).

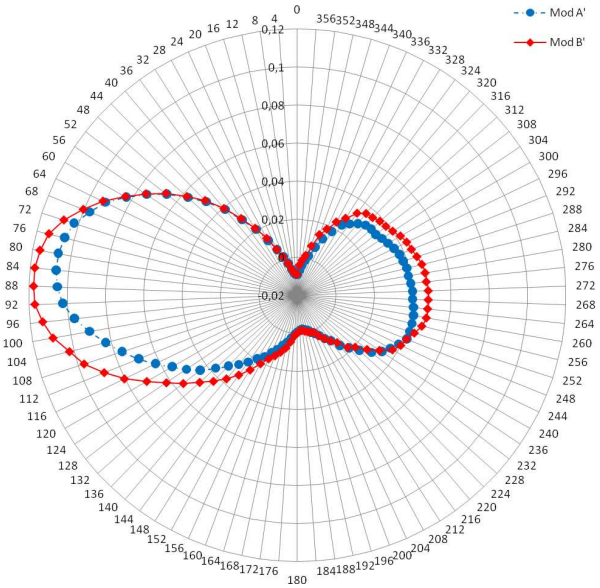

Fig. 15 Validation model.Effect of grid resolution on the instantaneous torque for a single-bladed rotor (turbulence model: k-ω SST). The difference between upwind and downwind blade performances can be noted

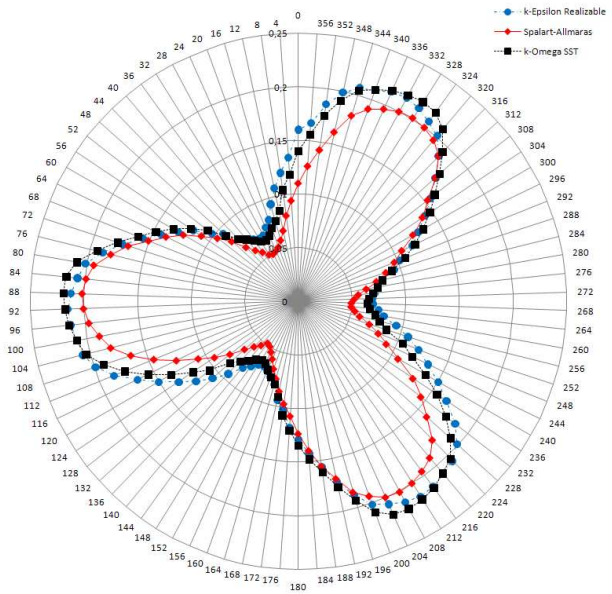

Fig. 16 Validation model.Effect of turbulence model on the instantaneous torque for a three-bladed rotor

Figs. 15 and 16 show the evolution of the instantaneous torque coefficient, defined as:

$$C_T(\theta) = T(\theta) / (\tfrac{1}{2} \rho A R V_\infty^2) \quad (4)$$

A function of the azimuthal position for two different meshes and for the three adopted turbulence models.

In order to fully appreciate even small variations of airfoil sections, a fine enough mesh to resolve the laminar sub layer was required for the boundary layer analysis settings.

The optimal grid resolution was selected on the basis of a better distribution of the blade y+ parameter. This parameter is a mesh-dependent dimensionless distance that quantifies the degree of wall layer resolution, in formulas:

$$y^+ = \rho u_\tau y / \mu \quad (5)$$

where ρ is air density, u_τ is the friction velocity, y the cell distance from the blade profile and μ is the dynamic viscosity.

Enhanced Wall Treatment k-ε Realizable proved to be the best turbulence model, mainly because of very poor sensitivity to grid dimension.

The temporal discretization has been achieved by imposing a time step equal to the lapse of time the rotor takes to make a 1° rotation. An improved spatial-discretization simulation did not show any significant variation.

The four analyzed models have kept some common points with the validation model, particularly as far as the chord length and the rotor radius are concerned. The blade-spoke connection point has been changed, since it had been placed in the centre of pressure of the profile, corresponding to 25% of the chord length behind the blade leading edge, while in the validation model it had been placed close to 50%. The analysis of the impact of this variation on the parameter y+ showed no significant effect, mainly due to the fact that in fast rotating machines, the values of blade relative velocity are determined primarily by the angular velocity of the rotor itself and to a lesser extent by the speed of undisturbed air flow.

Also the external size of the computational domain was changed: in the validation model the Wind Tunnel sub-grid had to reproduce the geometry of the wind tunnel. In order to avoid blockage effects due to the proximity to wind tunnel walls, the computational domain for the five helical models has been enlarged, as described in the previous section, allowing to analyze the behavior of the rotor in an open flow field. This additional change from validation model was limited to the outer portions of the computational domain and it was therefore considered negligible with respect to the values of blade y+.

The commercial CFD package used was Fluent 6.3.26, which implements 3-D Reynolds-averaged Navier-Stokes equations using a finite volume-finite element based solver. The fluid was assumed to be incompressible, being the maximum fluid velocity on the order of 60 m/s.

As a global convergence criterion, each simulation was run until the difference between two following periods of revolution, corresponding to a rotation of 120° due to rotor three-bladed geometry, was lower than 1%. Residuals convergence criterion for each single time step was set to 10^{-5}. The simulations, performed on a 8 processor, 2.33 GHz clock frequency computer, have been run until the instantaneous torque values showed a deviation of less than 1% compared with the corresponding values of the previous period. Total CPU time has been about 3 days for each simulation.

VI. Results and Discussion

Fig. 17 represents the average power coefficients for the three analyzed models, defined as:

$$C_p = P / (\tfrac{1}{2} \rho A V_\infty^3) \quad (6)$$

for an incident wind speed of 9 m/s, as a function of the tip speed ratio, defined as:

$$TSR = \omega R / V_\infty \quad (7)$$

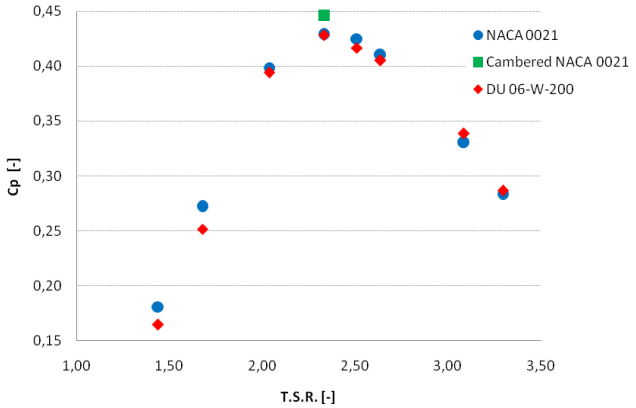

Fig. 17 Power curves for the three analyzed rotors (just the T.S.R.=2.33 value of cambered NACA 0021 was calculated)

The following remarks can be drawn:

- the three examined blade profile configurations show the same position of optimum tip speed ratio, being this parameter more connected with rotor solidity than with blade geometrical section;
- NACA 0021 rotor blade maximum value of Cp (0.429) is very close to DU 06-W-200 rotor blade corresponding value (0.428). This is in contrast to the results of Raciti Castelli and Benini [15], who registered a better performance for the DU 06-W-200 based rotor blade for a 2D numerical simulation of a turbine inside a wind tunnel. The reason of this discrepancy must be further investigated: nevertheless, it can be assumed to be connected with the blockage effect generated by the wind tunnel;
- cambered NACA 0021 rotor blade maximum value of Cp (0.447) is much higher (4.2%) than NACA 0021 corresponding value.

Figs. 18, 19 and 20 show the distribution of instantaneous torque coefficient as a function of azimuthal position of NACA 0021, cambered NACA 0021 and DU 06-W-200 rotor blade configuration, for a single rotor blade and for optimum tip speed ratio (TSR = 2.33).

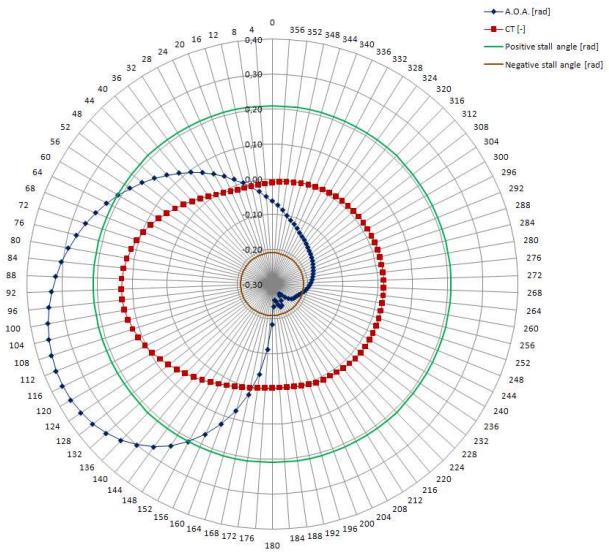

Fig. 18 Evolution of torque coefficient and of angle of attack as a function of blade azimuthal position for a single rotor blade (NACA 0021)

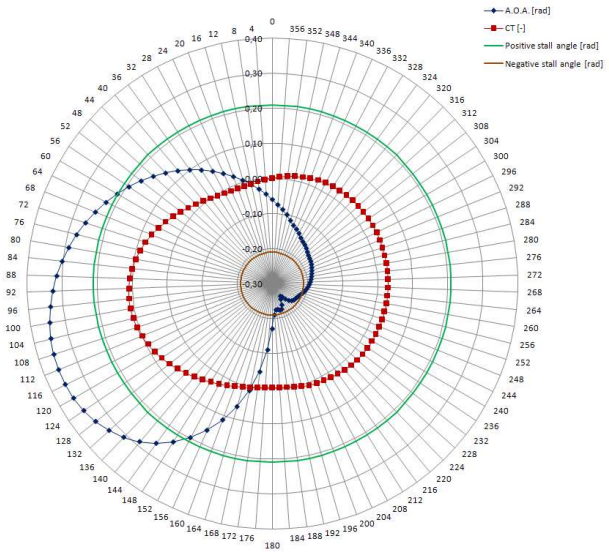

Fig. 19 Evolution of torque coefficient and of angle of attack as a function of blade azimuthal position for a single rotor blade (cambered NACA 0021)

Fig. 21 shows a comparison between the angles of attack for NACA 0021, cambered NACA 0021 and DU 06-W-200 rotor blade configuration as a function of azimuthal position, for optimum tip speed ratio (TSR = 2.33).

Fig. 22 shows a comparison between the torque coefficients of NACA 0021, cambered NACA 0021 and DU 06-W-200 rotor blade configuration as a function of azimuthal position, for optimum tip speed ratio (TSR = 2.33).

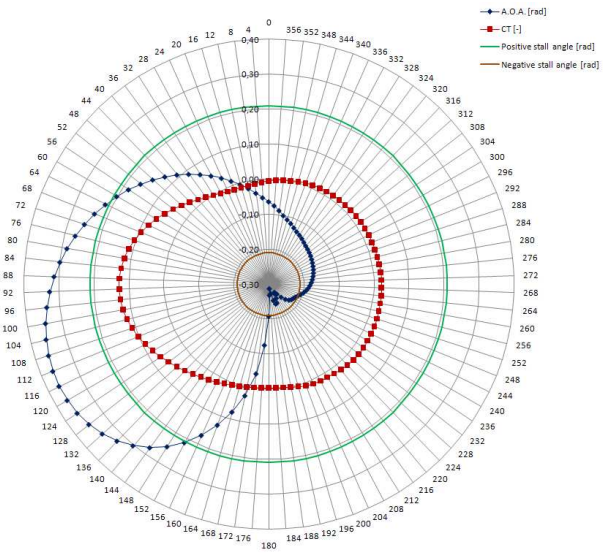

Fig. 20 Evolution of torque coefficient and of angle of attack as a function of blade azimuthal position for a single rotor blade (DU 06-W-200)

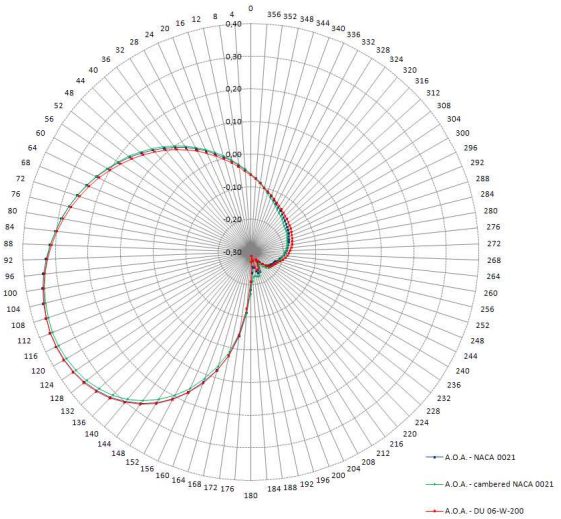

Fig. 21 Comparison between instantaneous angles of attack as a function of azimuthal position for the three analyzed models

The angle between the relative velocity and the tangent to the blade trajectory at each azimuthal position was also determined as:

$$\alpha = \text{arctg}\,[U \sin\gamma / (U \cos\gamma - U_t)] \quad (8)$$

being:

$$\gamma = \theta - \delta \quad (9)$$

$$\delta = \text{arctg}\,(U_y/U_x) \quad (10)$$

as proposed by Raciti Castelli et al. [16]. For further information on the adopted performance analysis, based upon

a simplified aerodynamic model, consisting in the analysis of kinematic and dynamic quantities every 4° rotor azimuthal position along blades trajectory, see [16].

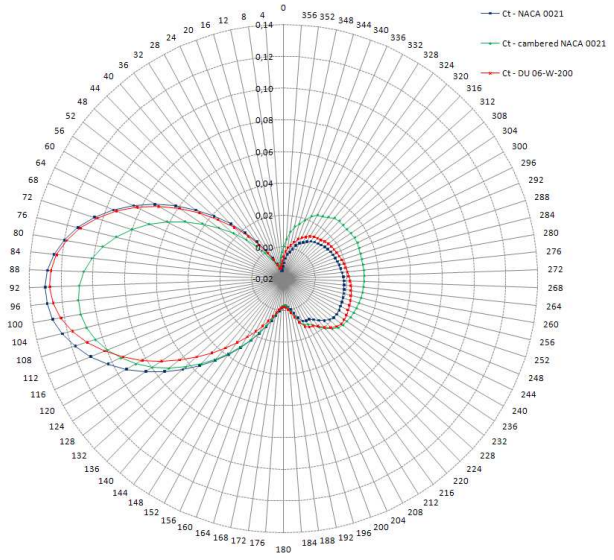

Fig. 22 Comparison between instantaneous torque coefficient as a function of azimuthal position for the three analyzed models

Once more, it can be clearly seen that torque values generated by cambered NACA 0021 blade profile are higher than those obtained from NACA 0021 and DU 06-W-200 rotor blade configurations, being these values the algebraic sum of each single blade contribution. It can be also noticed that, for upwind azimuthal positions cambered 0021 NACA performance is slightly lower if compared to the other two candidate airfoils, but for downwind azimuthal position the situation is quite the opposite and the overall balance is thus in favor of the cambered blade section.

VII. Conclusions And Future Work

In this paper a model for the evaluation of energy performance and aerodynamic forces acting on a small straight bladed Darrieus type vertical axis wind turbine depending on blade geometrical section has been developed, based on an analytical code coupled to a solid modeling software which was linked to a finite volume CFD code for the calculation of rotor performance.

The obtained results, based on three candidate blade section architectures, which are characterized by a conventional NACA 0021 blade profile and a newly developed DU 06-W-200 non-symmetric profile and a cambered NACA 0021 airfoil, demonstrate the better performance of the latter. The higher cambered NACA 0021 overall aerodynamic performance (up to nearly 4% with respect to the other two candidate airfoils) is due to an increased blade performance during downwind operation.

Further work should be performed in order to complete the power curve for the cambered NACA airfoil. Also the different behavior of a DU 06-W-200 based rotor for wind-tunnel and open-field conditions should be further investigate, in order to assess the validity of wind tunnel tests for VAWT performance prediction.

Nomenclature

A [m^2]	rotor swept area
c [mm]	blade chord
C_p [-]	rotor power coefficient
c_R [-]	chord to radius ratio
$C_T(\theta)$ [-]	rotor instantaneous torque coefficient
D [mm]	rotor diameter
H [mm]	rotor height
H_{domain} [mm]	wind tunnel height
N [-]	number of blades
P [W]	rotor power
R [mm]	rotor radius
R_b [mm]	chord radius with respect to rotor axis
u_τ [m/s]	tangential wall velocity
V [m/s]	wind velocity at test section
V_∞ [m/s]	unperturbed wind velocity at computational domain entrance
$V_{test\ section}$ [m/s]	wind velocity at rotor test section
V_∞ [m/s]	wind velocity at computational domain entrance
$T(\theta)$ [Nm]	rotor instantaneous torque
T.S.R. [-]	tip speed ratio
U [m/s]	absolute wind velocity at blade position
U_t [m/s]	blade tangential speed at blade position
U_x [m/s]	absolute wind velocity at blade position, component along x axis
U_y [m/s]	absolute wind velocity at blade position component along y axis
W_{domain} [mm]	computational domain width
y [m]	wall-grid centroid distance
y^+ [-]	blade y-plus
α [°]	blade angle of attack
ε_{sb} [-]	solid blockage
δ [°]	angle between absolute wind velocity at blade position and unperturbed wind direction
γ [°]	angle between absolute wind velocity at blade position and blade translational speed at blade position
θ [°]	blade azimuthal coordinate
μ [Pa·s]	air dynamic viscosity
ρ [kg/m^3]	unperturbed air density (assumed 1.225)
σ [-]	rotor solidity
ω [rad/s]	rotor angular velocity

References

[1] Sheldal, R. E., Klimas, P. C., "Aerodynamic Characteristics of Seven Symmetrical Airfoil Sections Through 180-Degree Angle of Attack for Use in Aerodynamic Analysis of Vertical Axis Wind Turbines", *SAND80-2114*, Unlimited Release, UC-60.

[2] Stathopoulos, T., "Wind Effects on People", *Proceedings of the International Conference on Urban Wind Engineering and Building Aerodynamics – Impact of Wind Storm on City Life and Built Environment*, COST Action C14, Von Karman Institute, Rode-Saint-Genèse (Belgium), 2004.
[3] Jensen, A. G., Franke, J., Hirsch, C., Schatzmann, M., Stathopoulos, T., Wisse, J., Wright, N. G., "CFD Techniques – Computational Wind Engineering", *Proceedings of the International Conference on Urban Wind Engineering and Building Aerodynamics – Impact of Wind and Storm on City Life and Built Environment* – Working Group 2, COST Action C14, Von Karman Institute, Rode-Saint-Genèse (Belgium), 2004.
[4] Paraschivoiu, I., *Wind Turbine Design: With Emphasis on Darrieus Concept*, Polytechnic International Press, Montreal, 2002.
[5] Johnston. S. F. (Editor), *Proceedings of the Vertical-Axis Wind Turbine (VAWT) Design Technology Seminar for Industry*, April 1-3, 1980, Sandia National Laboratories, SAND80-0984, August 1980.
[6] Saeed, F., Paraschivoiu, I., Trifu, O., "Inverse Airfoil Design Method for Low-Speed Straight-Bladed Darrieus-Type VAWT Applications", *7th World Wind Energy Conference 2008: Community Power*, Kingston, Ontario, Canada June 24-26th, 2008.
[7] Claessens, M. C., *The Design and Testing of Airfoils for Application in Small Vertical Axis Wind Turbines*, M.Sc. Thesis, Faculty of Aerospace Engineering, delft University of Technology, The Netherlands, November 9, 2006.
[8] Kadlec, E. G., "Characteristics of Future Vertical Axis Wind Turbines", *Sandia National Laboratories Report SAND79-1068*, Nov. 1982;
[9] Strickland, J. H., "The Darrieus Turbine: A Performance Prediction Model Using Multiple Streamtube", *SAND75-0431*.
[10] Simao Ferreira, C. J., Bijl, H., van Bussel, G., van Kuik, G., "Simulating Dynamic Stall in a 2D VAWT: Modeling Strategy, Verification and Validation with Particle Image Velocimetry Data", *The Science of Making Torque from Wind, Journal of Physics: Conference Series 75*, 2007.
[11] Bradshaw, P., *Experimental Fluid Mechanics*, Cambridge University Press, 1964.
[12] Fluent Inc., *Fluent User's Manual*, pp. 52, 54, 59, 71, 143.
[13] Cummings, R.M., Forsythe, J.R., Morton, S.A., Squires, K.D., "Computational Challenges in High Angle of Attack Flow Prediction", 2003, *Progr Aerosp Sci 39*(5):369-384;
[14] Raciti Castelli, M., Ardizzon, G., Battisti, L., Benini, E., Pavesi, G., "Modeling Strategy and Numerical Validation for a Darrieus Vertical Axis Micro-Wind Turbine", *IMECE2010-39548*.
[15] Raciti Castelli, M., Benini, E., "Comparison of Two Airfoil Sections for Application in Straight-Bladed Darrieus VAWT", submitted for publication to: *World Academy of Science, Engineering and Technology* on September 28, 2011.
[16] Raciti Castelli, M., Englaro, A., Benini, E., "The Darrieus Wind Turbine: Proposal for a New Performance Prediction Model Based on CFD", *Energy 36* (2011) 4919-4934.